Doxorubicin-loaded dual-functional hyaluronic acid nanoparticles: Preparation, characterization and antitumor efficacy *in vitro* and *in vivo*

GUIXIANG TIAN[1,2*], XIUE SUN[2*], JINGKUN BAI[1], JINHUA DONG[1,3], BO ZHANG[4], ZHIQIN GAO[1,3] and JINGLIANG WU[1,3]

[1]School of Bioscience and Technology; [2]Department of Psychology; [3]Key Laboratory of Biological Medicine in Universities of Shandong Province; [4]School of Pharmacy, Weifang Medical University, Weifang, Shandong 261053, P.R. China

Received April 2, 2018; Accepted October 10, 2018

DOI: 10.3892/mmr.2018.9687

Abstract. A novel GHH copolymer was synthesized using hyaluronic acid modified with glycyrrhetinic acid and L-histidine (His), and doxorubicin-loaded GHH nanoparticles (DOX/GHH) were prepared for liver-targeted drug delivery and pH-responsive drug release. In the present study, GHH nanoparticles were characterized, and their pH-responsive behaviors were evaluated at different pH levels. The antitumor effect of the DOX/GHH nanoparticles was investigated *in vitro* and *in vivo*. Results showed that the DOX/GHH nanoparticles were spherical, and the particle sizes ranged from 238.1 to 156.7 nm with an increase in the degree of substitution of His. The GHH nanoparticles were obviously internalized into human hepatoblastoma cells. *In vitro* cytotoxicity assay results showed that the DOX/GHH nanoparticles exhibited a dose-dependent antitumor effect. Compared with free DOX, the DOX/GHH nanoparticles displayed higher antitumor efficacy. These results indicate that GHH nanoparticles could be a promising nano-delivery carrier of hydrophobic drugs for liver-targeted therapy.

Correspondence to: Ms. Guixiang Tian, Department of Psychology, Weifang Medical University, 7166 Baotong West Street, Weifang, Shandong 261053, P.R. China
E-mail: gxtian2008@163.com

Dr Jingliang Wu, School of Bioscience and Technology, Weifang Medical University, 7166 Baotong West Street, Weifang, Shandong 261053, P.R. China
E-mail: jlwu2008@163.com

*Contributed equally

Key words: hyaluronic acid, nanoparticles, liver-targeting, pH-responsive

Introduction

Liver cancer is the third leading cause of death from cancer worldwide. To date, chemotherapy is the primary treatment for liver cancer. However, most anticancer drugs cause systemic toxicity and side effects to patients due to their poor specificity (1,2). Recently, nano-sized drug delivery systems have been widely applied for cancer treatment through targeted delivery with reduced adverse effects (3,4). Natural copolymers, such as chitosan (5,6), hyaluronic acid (HA) (7,8), and other polysaccharides (9,10), have been well-recognized as nanoparticles in drug delivery and cancer therapy.

HA, a natural linear and negatively charged polysaccharide present in extracellular matrices, has been used as a potential tumor-targeting moiety because of its biocompatibility, biodegradability and overexpression of HA-binding receptors on tumor cells. Drug-loaded nanocarriers based on HA conjugates, such as doxorubicin (11,12), paclitaxel (13,14) and siRNAs (15,16), have been found to exhibit enhanced targeting ability in various tumor cells.

HA can be modified by other moieties, such as galactose (17), glycyrrhetinic acid (GA) (18-20), and various ligands, to improve the selectivity of nanoparticles based on HA copolymers. This strategy considerably increases the accumulation of drugs in tumor cells and results in lower toxicity and fewer side effects than traditional chemotherapy (21). Meanwhile, GA has attracted increased attention as it can specifically bind with GA-receptors in hepatocyte membranes and is less expensive than antibodies. GA-modified drug-loaded nanoparticles can improve anti-hepatoma efficacy and reduce toxic side effects (22-24).

In the present study, we prepared a novel DOX/GHH drug delivery system. The prepared DOX/GHH nanoparticles achieved the dual-function of liver-targeted delivery via GA receptor-mediated endocytosis and drug release from lysosomes via protonation of the imidazole group of His (Fig. 1). First, HA polymers modified by GA and His were synthesized. Then, the physicochemical characteristics of the GHH nanoparticles were investigated. Finally, the anti-hepatoma effect of DOX/GHH nanoparticles was evaluated *in vitro* and *in vivo*.

Materials and methods

Materials. Hyaluronic acid (HA) (MW, 80 kDa) was purchased from Bloomage Freda Biopharm Co., Ltd. (Jinan, China). L-histidine (His) was purchased from Sinopharm Chemical Reagent Co., Ltd. (Shanghai, China). Glycyrrhetinic acid (GA) was acquired from Meheco Tianshan Pharm Co., Ltd. (Beijing, China). DOX·HCl was purchased from Shanghai Sangon Biomart Co., Ltd. (Shanghai, China).

4-(4,6-Dimethoxy-1,3,5-triazin-2-yl)-4-methylmorpholinium chloride (DMT-MM), pyrene and MTT was procured from Sigma-Aldrich (Merck KGaA, Darmstadt, Germany). RPMI-1640 medium was purchased from Beijing BioDee Biotechnology Co., Ltd. (Beijing, China). All chemicals were of analytical grade.

Cell cultures. Human hepatic cell line (HepG2) was obtained from the China Center for Type Culture Collection (Wuhan, China), while murine HCC cells (H22) were gifted by the Institute of Immunopharmacology and Immunotherapy of Shandong University (Jinan, China). Both cell lines were cultured in RPMI-1640 medium, supplemented with 10% fetal bovine serum (FBS), 1% penicillin and 1% streptomycin at 37˚C in an environment containing 5% CO_2.

Animals. Female BALB/c mice (weight: 18±2 g) were supplied by the Experimental Animal Center of WeiFang Medical University (Weifang, China). In total 36 mice were used for *in vivo* imaging and antitumor efficacy experiments. The animals were fed at 25±2˚C in the institutional animal house facility (relative humidity: 40-70%, 12-h/d light dark cycle), with a standard diet and allowed water *ad libitum*.

Synthesis of GHH copolymers. GHH copolymers were synthesized through a two-step reaction. First, GA solution in methanol was activated to form an active ester in the presence of DMT-MM. The active ester solution was evaporated to remove methanol, and slowly added to an ethylene diamine solution under stirring at room temperature for 24 h. Then, the diamine-modified GA (GA-NH_2) was obtained after purification by column chromatography. The GA-HA conjugate was synthesized by the chemical modification of GA–NH_2 to the backbone of HA (70 kDa). Second, the GA-HA conjugate was dissolved in formylamine before DMT-MM was slowly added. Then, His was slowly added to the GA-HA solution, followed by stirring at room temperature for 24 h. After filtration, the solution was freeze-dried to obtain GHH copolymers. The chemical structures of the GHH conjugates were determined by ^{1}H NMR (JNM ECP-600, JEOL, Japan) by dissolving the conjugate in D_2O.

Characterizations of the GHH copolymers. Pyrene was used as a probe to evaluate the aggregation behavior of the GHH copolymer via fluorescence spectrophotometry (25). In brief, pyrene was dissolved in ethanol at a concentration of $6.0x10^5$ M, and the solution was shaken for 24 h to evaporate the ethanol at 60˚C. Different concentrations of GHH solutions were added to each tube, and the pyrene concentration was maintained at $6.0x10^{-7}$ M. The fluorescence spectra of pyrene were measured with an RF-5301PC fluorescence spectrophotometer (Shimadzu Co., Kyoto, Japan). The variation in intensity ratios from the first peak (372 nm) to the third peak (383 nm) was sensitive to the polarity of the microenvironments where pyrene was located. The I_{372}/I_{383} fluorescence ratio of pyrene was analyzed for critical micelle concentration (CMC) calculation. The CMC legend was used to estimate the threshold concentration of the self-aggregated nanoparticle formation, which was important for investigating the self-aggregation behavior and structural stability of micelles.

The stability of the GHH micelles was tested by dynamic light scattering spectrophotometry (Malvern Instruments Ltd., Malvern, UK). In brief, the solution containing the GHH micelles was mixed with RPMI-1640 medium containing 10% FBS. Then, the mixture solution was maintained in a shaking water bath at 100 rpm and 37˚C. All measurements were conducted at a wavelength of 635 nm at 25˚C. The experiment was repeated for three samples.

pH-responsive behavior of the GHH nanoparticles. The GHH nanoparticles were dissolved in PBS solutions with different pH values (7.4, 7.0, 6.8, 6.4, 6.0 and 5.0). The concentration of the GHH nanoparticles was maintained at 1 mg/ml. pH-induced changes in particle size were examined by Malvern Zetasizer Nano ZS90. All measurements were conducted in triplicate.

Preparation of DOX-loaded nanoparticles. DOX/GHH nanoparticles were prepared through a modified dialysis method as described previously (26). In brief, GHH copolymers were dissolved in formamide. DOX·HCl was dispersed in N,N-dimethylformamide in the presence of triethylamine (TEA) (M_{TEA}:M_{DOX}=1.3). Then, the latter was added dropwise to the GHH solution by stirring. Then, a dialysis bag [molecular weight cut-off (MWCO) 3,500 kDa] was used for the dialysis of the mixed suspension against deionized water for the removal of unloaded drugs. Additionally, DOX-loaded HA-GA nanoparticles were prepared as control. DOX/HA-GA nanoparticles and DOX/GHH nanoparticles were obtained by freeze-drying the dialysis solution.

The drug loading capacity (DL) and entrapment efficiency (EE) of the GHH nanoparticles were evaluated using a UV-vis spectrophotometer at 479 nm. The DL and EE values were calculated using the following equations:

$$DL=W_S/W_T \times 100\% \quad EE=W_S/W_A \times 100\%$$

where W_S is the DOX weight in the nanoparticles, W_T is the total weight of the freeze-dried nanoparticles, and W_A is the feeding weight of DOX.

In vitro DOX release from the GHH nanoparticles. The *in vitro* pH-responsive release behavior of the DOX/GHH nanoparticles was investigated through a dialysis method (cut-off=3.5 kDa). In brief, the DOX/GHH nanoparticles were dissolved in PBS solution. Three solutions with different pH values (7.4, 6.8, and 5.0) were prepared. The dialysis bags were dialyzed against a fresh PBS solution (0.1 M; pH 7.4, 6.8 and 5.0) and placed in a shaking incubator with a stirring speed of 100 rpm at 37˚C.

At predetermined time intervals, the medium (4 ml) was withdrawn, and the same volume of fresh PBS solution was added. DOX concentration was measured with a UV-vis

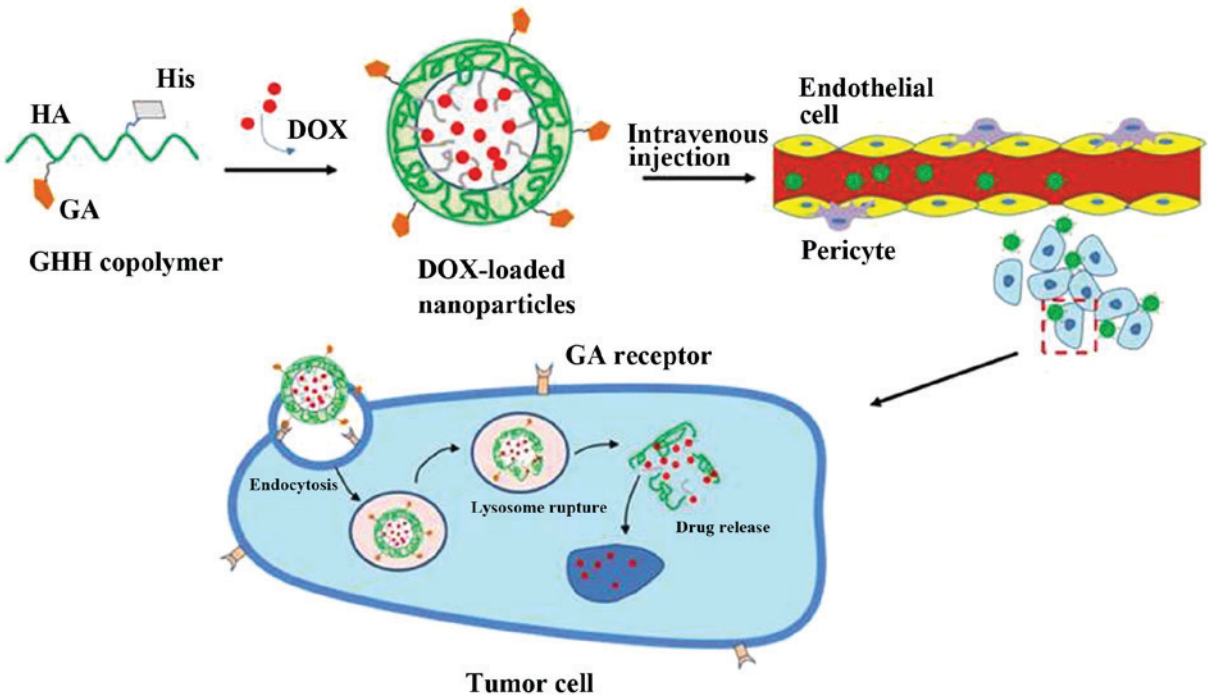

Figure 1. Schematic illustration of liver-targeting delivery and pH-triggered release of DOX from GHH nanoparticles. The illustration shows self-assembly, accumulation in tumor tissue and intracellular uptake of GHH nanoparticles as well as liposomal escape and pH-triggered drug release.

spectrophotometer at 479 nm. Cumulative DOX release percentage (Er) was calculated using the following equation:

$$Er(\%) = \frac{Ve\sum_{1}^{n-1} Ci + V_0 Cn}{m_{DOX}} \times 100\%$$

Where m_{DOX} is the amount of DOX in the nanoparticles, V_0 represents the whole volume of the release medium, C_i is the concentration of DOX in the medium, and V_e represents the volume of the replaced medium. The *in vitro* DOX release measurement was performed in triplicate at each pH value.

In vitro cytotoxicity of the DOX/GHH nanoparticles. The cytotoxicity of the blank nanoparticles and the DOX-loaded nanoparticles against HepG2 cells was tested by MTT assay as previously described (27). In brief, the HepG2 cells were seeded in 96-well plates ($5x10^3$ cells/well) and cultured overnight at 37˚C in a humidified atmosphere of 5% CO_2. Then, the cells were incubated with free DOX and DOX-loaded nanoparticles for 48 h at equivalent DOX concentrations of 0.01, 0.1, 1.0, 5.0 and 10.0 μg/ml. Cell viability was determined through MTT assay. The half maximal inhibitory concentration values (IC_{50}) of the different formulations were calculated in SPSS 17.0 (SPSS, Inc., Chicago, IL, USA). All measurements were performed in triplicate.

In vitro cellular uptake studies. To evaluate the targeting ability of the nanoparticles, the *in vitro* cellular uptake of the GHH nanoparticles was observed by fluorescence microscopy (IX51; Olympus Corporation, Tokyo, Japan). A FITC-labeled GHH copolymer was synthesized as previously reported (28). The HepG2 cells were seeded in 6-well plates ($5x10^4$ cells/ml) at 37˚C. When the cells reached 70-80% confluence, FITC-labeled GHH nanoparticles, DOX/HA-GA nanoparticles, or DOX/GHH nanoparticles (5 μg/ml of DOX) in serum-free medium were added and incubated at 37˚C. After 2 h of incubation, the cells were washed and fixed. DAPI staining (1:500; Sigma-Aldrich) was performed to visualize the nuclei of the HepG2 cells. Finally, the cellular uptake and intracellular distribution of the GHH nanoparticles were visualized by fluorescence microscopy, and the merged images were created with Image Pro Plus 6.0 (Media Cybernetics, Inc., Rockville, MD, USA).

In vivo near-infrared fluorescence imaging. The *in vivo* biodistribution of the GHH nanoparticles was monitored using DiR as a near-infrared fluorescence agent. Imaging of the DiR-loaded GHH nanoparticles was performed at pre-determined times (1, 2, 6 and 12 h), using the Xenogen IVIS Spectrum from Caliper Life Sciences (Waltham, MA, USA). The excitation and emission wavelengths selected were at 745 and 835 nm, respectively.

In vivo antitumor efficacy. H22 tumor-bearing mice were prepared to evaluate the antitumor efficacy of the DOX/GHH nanoparticles. The mice were subcutaneously injected at the right axillary space with 0.1 ml cell suspensions containing $1x10^6$ H22 cells. The mice were divided into five groups and treated with: i) normal saline (the control group), ii) blank GHH nanoparticles, iii) DOX, iv) DOX/HA-GA nanoparticles, and v) DOX/GHH nanoparticles. When the tumor volume reached 100 mm^3, each treatment was administered in an equivalent volume of 0.2 ml every other day. The three drug formulations were injected at a dose of 5 mg/kg body weight. Tumor volumes were observed for 14 days once per day. The individual tumor volume (V) was calculated by $V=(W^2xL)/2$, where the width (W) is the shortest tumor diameter, and the length (L)

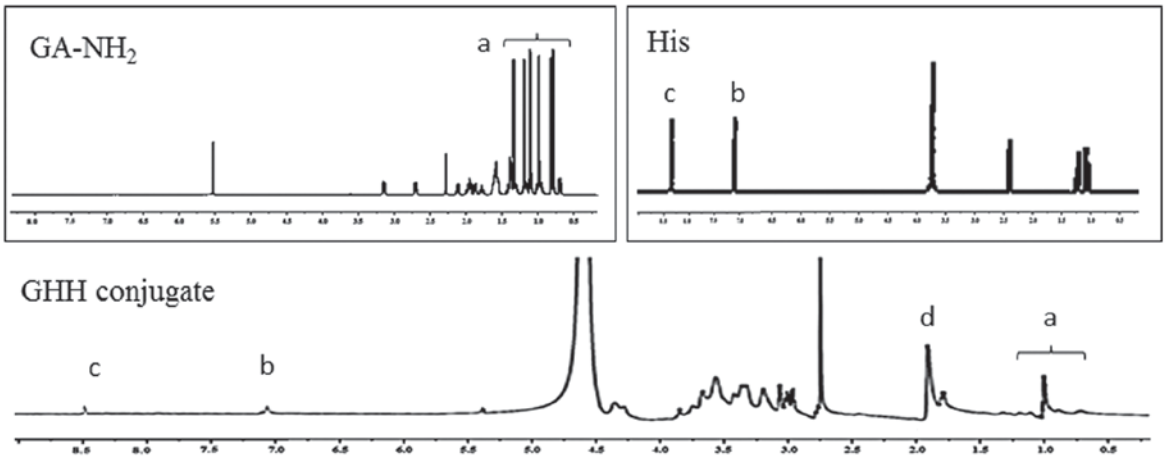

Figure 2. ^{1}H Nuclear magnetic resonance spectra of the GA-NH_2, His and GHH conjugate. (a) Peaks of GA-NH_2 at 0.64-1.5 ppm; (b) and (c) peaks of His at 7.11 and 8.44 ppm; (d) peaks of HA chain at 1.91 ppm.

is the longest tumor diameter. The values are presented as the mean ± standard deviation (SD) for groups of at least five animals. Finally, the mice were sacrificed by cervical vertebra dislocation after anesthesia using 10% chloral hydrate, and the tumors were removed.

Statistical analysis. All results are presented as mean ± SD, n=3 parallel samples. One-way analysis of variance was used to make comparison of several groups, and SNK-q test was used to make post hoc test. $P<0.05$ was considered to indicate a statistically significant difference.

Results

Synthesis and characterization of the GHH conjugates. The GHH copolymer was synthesized by coupling aminated GA and His to the HA backbone. The characteristic peaks of HA, GA-NH_2 and His were confirmed (Fig. 2). In this investigation, the characteristic peaks of the methyl and methylene groups (0.7-1.5 ppm) of GA, the *N*-acetyl group (1.91 ppm) of HA, and the imidazole ring (7.11 and 8.44 ppm) of His were confirmed. These results indicated that the GA-NH_2 and His groups were successfully introduced into HA copolymers owing to the presence of peaks at 0.6-1.5 ppm (peaks of GA-NH_2), 7.11 and 8.44 ppm (peaks of His) in the GHH conjugates.

The degree of substitution (DS) was estimated by UV measurement (λ=260 nm). The HA-GA conjugate (DS=5.8%) was selected as the candidate for further research because of its low particles size. His, a pH-responsive group, was successfully introduced to the HA backbone in the presence of DMT-MM. When the molar ratios between HA-GA and His were 1:3, 1:6 and 1:9, the DS values of His were 4.6, 8.6 and 10.2%, respectively, and the copolymers were designated as GHH-4, GHH-8 and GHH-10.

The CMC value is widely used to monitor the self-aggregation behavior of amphiphilic polymers and the structural stability of micelles *in vitro* and *in vivo*. The CMC values of the GHH conjugates with different DS values were measured with pyrene as the hydrophobic molecule. As shown in Fig. 3A, the fluorescence intensity ratio (I_{373}/I_{383}) was plotted, and the CMC was measured from the threshold concentration of the GHH copolymer. The CMC values of the GHH conjugate ranged from 0.024 to 0.089 mg/ml.

GHH nanoparticles were prepared by ultrasonic dispersion. The mean diameters of the GHH nanoparticles exhibited no significant changes over 7 days when stored under physiological conditions (RPMI-1640 medium, 37˚C), suggesting that the GHH nanoparticles were highly stable (Fig. 3B).

The pH-responsive behavior of the GHH copolymers was tested on the basis of particle size and zeta (ζ) potential at different pH values (Fig. 3C and D). At pH 7.0-7.4, the average particle size was nearly unchanged (148.7-158.6 nm), suggesting that the GHH nanoparticles were stable under physiological condition. The abrupt increases in mean particle size and particle diameter distribution were caused by a stepwise shift from pH 6.8 to 5.0. Fig. 3D demonstrates that the ζ potential increased when the pH was changed from 7.4 to 5.0 and remained negatively charged.

Formation and characterization of the DOX/GHH nanoparticles. DOX-loaded nanoparticles based on GHH copolymers were prepared through a simple ultrasonic method. When DOX was mixed with GHH nanoparticles at an initial ratio of 1:10, DOX was physically encapsulated in the GHH-4, GHH-8 and GHH-10 copolymers, and the resulting complexes were named DOX/GHH-4, DOX/GHH-8 and DOX/GHH-10, respectively. The mean particle sizes, ζ potential, EEs, and DLs of the different DOX-loaded nanoparticles are shown in Table I. The mean particle sizes and absolute values of the ζ potential decreased when the DS values of His increased. The DL and EE values of the DOX-loaded nanoparticles decreased when the DS of His increased. DOX/GHH-10 was chosen as the nanocarrier for further research due to its low particle size. As shown in Fig. 4A, DOX/GHH-10 has well-separated particles with a rather narrow size distribution. TEM micrograph shows that it was nearly spherical (Fig. 4B).

pH-responsive DOX release from GHH nanoparticles in vitro. *In vitro* DOX release from the DOX/GHH nanoparticles was measured at 37˚C. As shown in Fig. 5, a pH-responsive release profile was found in DOX release at the different pH values. The DOX-loaded nanoparticles were stable at pH 7.4 and

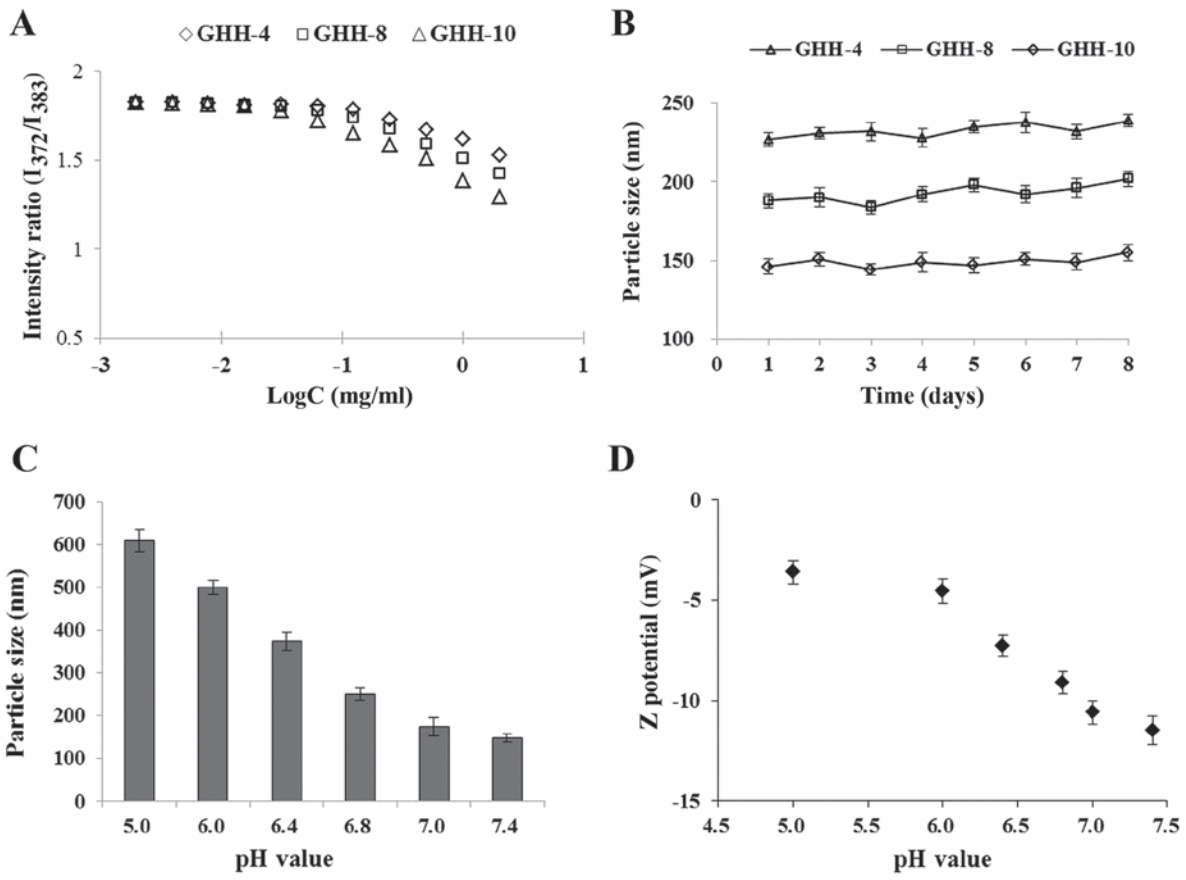

Figure 3. Characterization of the GHH nanoparticles: (A) CMC determination (B) stability analysis in RPMI-1640 medium, (C) particle size and (D) ζ potential at different pH values at 37˚C. Data represent mean ± standard deviation, n=3. CMC, critical micelle concentration.

released only 21.4% of DOX after 24 h. Under an extracellular tumoral condition (pH 6.8), 29.8% cumulative DOX was determined. However, at an intralysosomal pH of 5.0, the DOX release rate was much faster, with 58.9% of DOX released after 24 h.

In vitro cellular uptake of the DOX/GHH nanoparticles. The intracellular uptake of the GHH nanoparticles was evaluated by fluorescence microscopy. FITC was used as a fluorescence probe for tracking the distribution of GHH nanoparticles in the HepG2 cells. DAPI was regarded as a fluorescence marker for the visualization of the HepG2 cell nuclei. In Fig. 6A, green spots were observed in the cytoplasm after the cells were incubated with FITC-labeled nanoparticles, suggesting that the GHH nanoparticles were taken up by endocytosis of the HepG2 cells.

The cellular uptake of DOX from the GHH nanoparticles was analyzed with the autofluorescence of DOX. The distribution of DOX in the HepG2 cells was determined by obtaining the overlay of the fluorescent images. The results of cellular uptake after 1.5 h of incubation with the DOX/HA-GA or DOX/GHH nanoparticles are showed in Fig. 6B and C. Red spots (DOX) were observed in the HepG2 cells, indicating that DOX was released from the HA-GA nanoparticles or GHH nanoparticles. However, compared with the DOX/HA-GA nanoparticles, a larger amount of DOX from the GHH nanoparticles was distributed in the cytoplasm and nuclear regions.

In vitro cytotoxicity of the DOX/GHH nanoparticles. The cellular viability of blank GHH nanoparticles was investigated by MTT assay. The results demonstrated that cellular viability was over 85% after incubation with the blank nanoparticles for 48 h, indicating that the GHH conjugate exhibited no significant cytotoxicity with a concentration of up to 1 mg/ml, and could be used as carriers of antitumor drugs (Fig. 7A). The *in vitro* cytotoxicity levels of the DOX formulations were evaluated against the HepG2 cells. As demonstrated in Fig. 7B, free DOX, DOX/GA-HA nanoparticles and DOX/GHH nanoparticles exhibited dose-dependent cytotoxic effects after incubation for 48 h. The IC_{50} values of free DOX, DOX/GA-HA nanoparticles, and DOX/GHH nanoparticles were 1.32, 1.41 and 1.07 μg DOX equiv/ml, respectively.

In vivo imaging analysis. To investigate the liver-targeting capacity of the GHH nanoparticles, DiR-loaded micelles were prepared to analyze the biodistribution of GHH nanoparticles in mice by fluorescence imaging. As presented in Fig. 8, DIR was obviously accumulated in the liver and tumor. DiR-loaded GHH nanoparticles began to accumulate in the tumor at 1 h, reached the maximum fluorescent intensity at 6 h, and then declined gradually but was still detectable until 12 h.

In vivo antitumor efficacy. The *in vivo* anti-hepatoma efficacy of the DOX/GHH nanoparticles for H22 tumor-bearing mice was tested for 14 days. In Fig. 9, the blank GHH nanoparticle

Table I. Characterization of the DOX/GHH nanoparticles at pH 7.4 (n=3).

Nanoparticles	Diameter (nm)	PDI	ζ potential (mV)	EE (%)	DL (%)
DOX/GHH-4	238.1±9.4	0.197	-13.7±1.2	91.3±1.8	9.21±0.52
DOX/GHH-8	172.7±5.7	0.159	-11.2±0.9	88.7±2.1	8.92±0.47
DOX/GHH-10	156.7±8.6	0.137	-10.4±1.1	87.4±1.5	8.84±0.39

PDI, polydispersity index; EE, entrapment efficiency; DL, drug loading capacity.

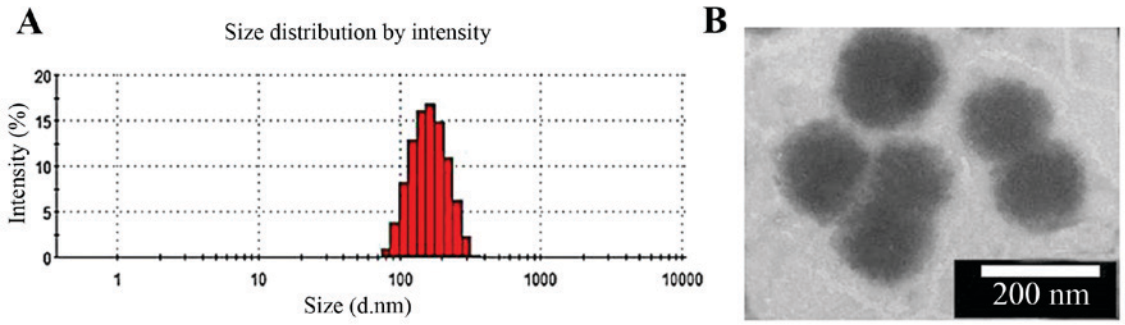

Figure 4. Characteristics of the DOX/GHH nanoparticles (DOX/GHH-10). (A) Particles size distribution and (B) transmission electron microscopy image. DOX, doxorubicin.

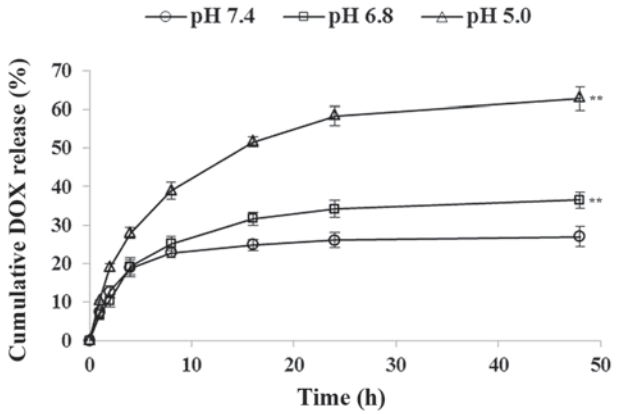

Figure 5. Release behavior of DOX from GHH nanoparticles at different pH values at 37˚C. Data represent mean ± standard deviation, n=3. (**P<0.01 vs. pH 7.4). DOX, doxorubicin.

treatment results showed an equivalent increase in tumor size with the control group. This result suggested that the blank nanoparticles had no antitumor efficacy. As expected, the tumor sizes of the three DOX formation groups were significantly smaller than that of the saline group. Notably, compared with the free DOX group, the groups containing the DOX/HA-GA and DOX/GHH nanoparticles had considerably higher antitumor efficacy. To investigate the *in vivo* antitumor activity, we extracted the tumors from the five groups of H22 cell-bearing mice (Fig. 9). The results demonstrated that the tumor sizes from the three DOX treatments were considerably smaller than those in the control group, indicating significant antitumor effect. Notably, the DOX/GHH nanoparticle groups showed higher inhibition efficiency than the two other DOX treatment groups.

Discussion

Liver-targeting nanoparticles can deliver antitumor drugs to liver cancer tissues, reducing drug side effects. Glycyrrhetinic acid (GA), an aglycone of glycyrrhizin, can specifically bind to receptors on the membrane of liver cancer cells. This characteristic makes GA a suitable candidate for the development of a liver-targeted delivery nanocarrier (29,30). In our previous study, pH-responsive nanoparticles based on His-modified HA polymers were prepared and used as nanocarrier for doxorubicin (DOX) delivery against MCF-7 cells (28). In the present study, we prepared dual-functional GHH nanoparticles that were expected to achieve the liver-targeted delivery of DOX and efficient escape from lysosomes. The critical micelle concentration (CMC) value is widely used to monitor the self-aggregation behavior of amphiphilic polymers and structural stability of micelles in vitro and in vivo (31). The CMC values of the GHH conjugate ranged from 0.024 to 0.089 mg/ml, indicating that the structural integrity of the conjugate was improved because of the strong hydrophobic interactions in the inner core of the GHH conjugate at a low copolymer concentration. At a low CMC value, the stability of the self-assembled micelles in the bloodstream may be retained as dissociation is prevented under highly diluted conditions (32).

The particle size and ζ potential of the GHH nanoparticles were increased as the pH values decreased from 7.4 to 5.0. This phenomenon might be explained by the introduction of the ionizable imidazole ring of His. These imidazole groups are protonated at an acidic pH, resulting in the increased size of the GHH nanoparticles. Furthermore, the shells of the nanoparticles are covered by negatively charged HA chains, and the protonated imidazole groups of His increase at a low pH, resulting in change in the surface charge of the GHH nanoparticles (33).

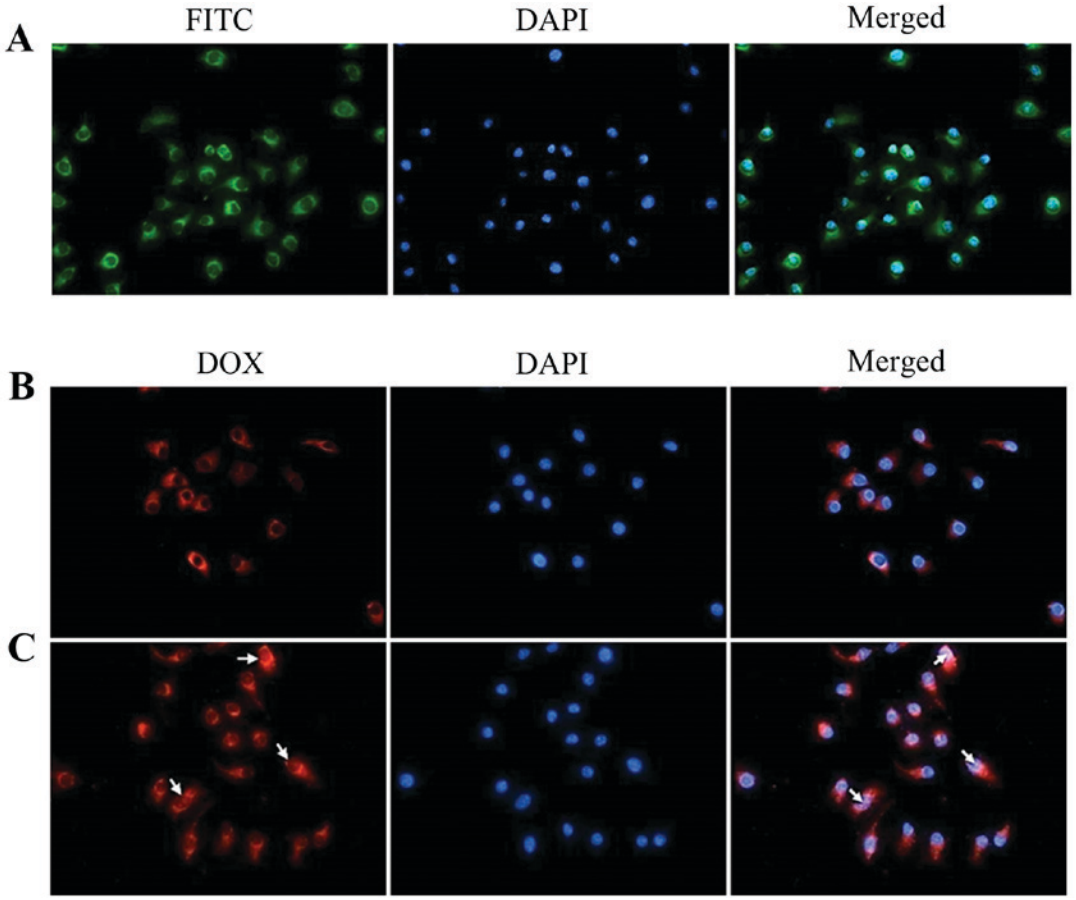

Figure 6. Fluorescence micrographs of HepG2 cells incubated with (A) FITC-labeled nanoparticles, (B) DOX/GA-HA nanoparticles and (C) DOX/GHH nanoparticles. For each panel, the images from left to right show the intracellular distribution of nanoparticles (FITC, green) or DOX (red), cell nuclei stained by DAPI (blue) and overlays (Merged) of all images. DOX, doxorubicin; FITC, fluorescein isothiocyanate.

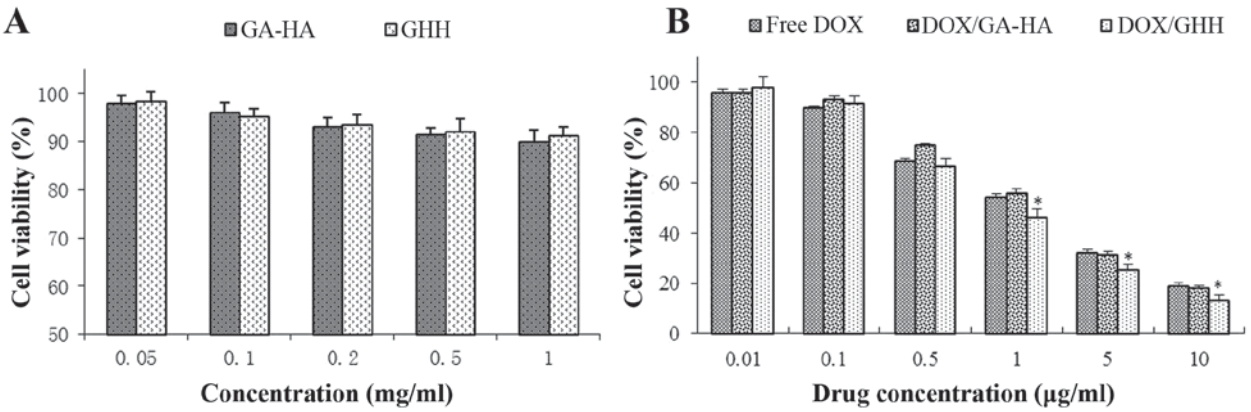

Figure 7. Viability of HepG2 cells treated with (A) blank nanoparticles and (B) free DOX, DOX/GHH nanoparticles, or DOX/GA-HA nanoparticles for 48 h (n=3) (*P<0.05 vs. DOX). DOX, doxorubicin.

Table I shows that the mean particle sizes and absolute values of the ζ potential of the DOX/GHH nanoparticles decreased with the increase in the DS of the His group. This trend might be due to the introduction of more His molecules, resulting in the formation of more compact hydrophobic cores and the reduction in the number of carboxyl groups in the GHH copolymers. Moreover, the modification of more His molecules could form tighter cores in GHH nanoparticles, resulting in a weak repulsion between DOX and the hydrophobic core (34).

To investigate the release behavior of the DOX-loaded nanoparticles under physiological conditions, a tumor acidic microenvironment, and an intralysosomal pH, we measured the *in vitro* DOX release of the DOX/GHH nanoparticles at pH 7.4, 6.8 and 5.0, respectively. The DOX release rates were significantly differed at pH 7.4 and 5.0 ($P<0.05$). The results were due to the protonated imidazole ring in the core of His at pH 5.0, which is below the pKa of the histidyl imidazole ring (pH, 6.5). However, no significant difference ($P>0.05$)

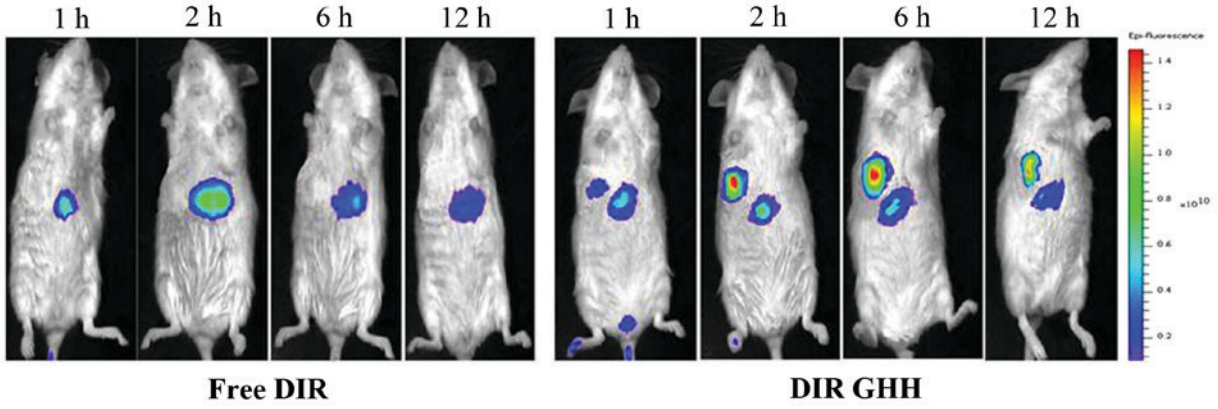

Figure 8. Real-time NIR images of H22 tumor-bearing mice after injection of free DiR and DiR-GHH micelles. NIR, near-infrared; DiR, 1, 1'dioctadecy-3, 3, 3, tetramethylindotricarbocyanine iodide.

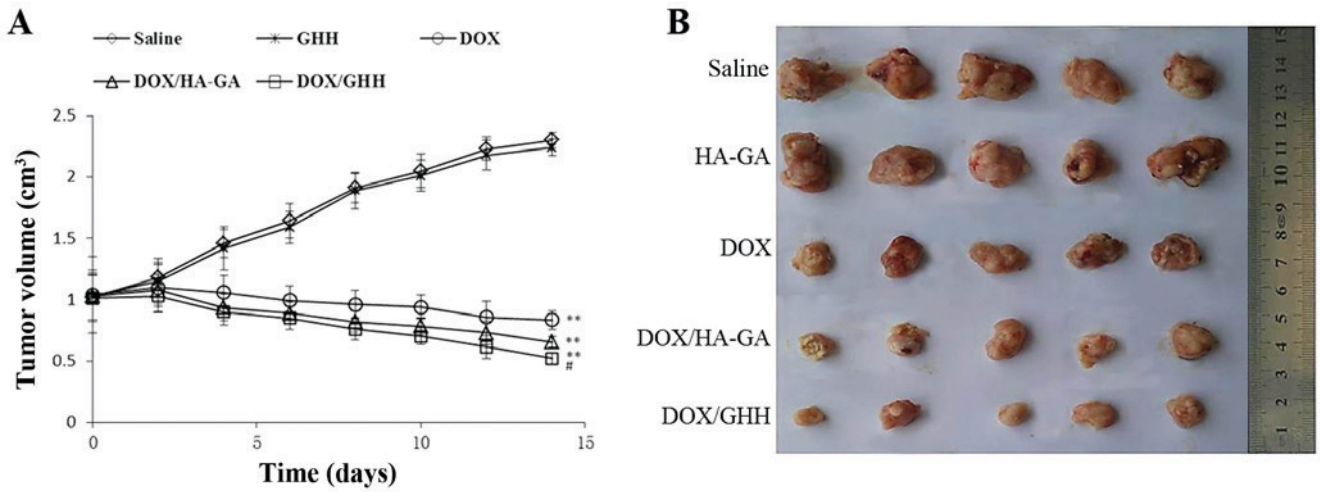

Figure 9. (A) Time-dependent tumor growth profile of H22-bearing mice administered with saline, black GHH nanoparticles, free DOX, DOX/GA-HA nanoparticles and DOX/GHH nanoparticles, respectively. The mean ± SD of the tumor volumes from five mice were provided. Data represent mean ± SD, n=5 (**P<0.01 vs. control; $^{\#}$P<0.05 vs. DOX). (B) Excised tumor images after antitumor therapy. SD, standard deviation; DOX, doxorubicin.

was observed between pH 7.4 and 6.8. The pH-responsive drug release behavior showed that the rate and amount of DOX release from the nanoparticles increased as the pH was decreased from 7.4 to 5.0. Under physiological conditions (pH 7.4), the micelles had a stable hydrophobic cores composed of GA and His, and DOX was released slowly via a diffusion mechanism. At pH 6.8, the release rates of DOX increased due to the slight swelling of the micelles owing to the partial protonation of the imidazole ring of His. Under an intralysosomal condition (pH 5.0), the majority of the imidazole rings were protonated, and the charged imidazole groups repelled each other and moved out of the hydrophobic core, which caused the marked swelling and demicellization of the GHH micelles. Luo and Jiang also reported that drugs are released from pH-responsive nanoparticles/vesicles through the swelling-demicellization–releasing mechanism (35).

MTT assay was used to evaluate the cytotoxicity of the DOX/GHH nanoparticles. The IC_{50} value of the DOX/GHH nanoparticles was lower than that of the DOX/HA-GA nanoparticles. These results indicated that the DOX/GHH nanoparticles escaped quickly from lysosomes and rapidly released DOX into the cytoplasm through a proton sponge effect, which enhanced the cytotoxicity levels (36,37). Meanwhile, compared with the free DOX group, the DOX/GHH nanoparticle group showed higher antitumor efficacy. A possible explanation is that GA-receptor-mediated endocytosis inhibits P-glycoprotein-mediated drug efflux, resulting in its high antitumor efficacy (38,39). The *in vivo* antitumor efficacy of the DOX/GHH nanoparticles was investigated against H22 tumor-bearing mice. Relative to the control group, the three drug treatment groups had antitumor efficacy. Notably, the DOX-loaded nanoparticles had considerably higher antitumor efficacy than free DOX. The results might be due to the fact that the nano-delivery system improves DOX accumulation in tumor cells via the enhanced permeability and retention effect (40,41). Importantly, the GHH nanoparticle treatment group showed a higher antitumor effect than the DOX/HA-GA nanoparticles. A possible explanation is that the DOX released from the GHH nanoparticles easily escaped from the lysosomes after the introduction of His, resulting in their higher antitumor efficacy (42).

In conclusion, a novel GHH copolymer was synthesized, and self-assembled dual-functional nanoparticles were prepared for the liver-targeted delivery of DOX. *In vitro*

release studies showed that the GHH nanoparticles released DOX in a pH-responsive manner. Cellular uptake results indicated that the introduction of His to the HA backbone substantially increased the release rate of DOX from the lysosomes of HepG2 cells. Moreover, *in vivo* antitumor activity analysis showed that the GHH nanoparticles exhibited higher antitumor efficacy than free DOX or DOX/HA-GA nanoparticles. All of these results demonstrated that GHH copolymers are biocompatible and exhibit great potential as liver-targeted and pH-responsive delivery systems in the prevention and treatment of liver cancer.

Acknowledgements

Not applicable.

Funding

This study was supported by the National Natural Science Foundation of China (grant no. 81274093), the Higher Education Science and Technology Project of Shandong Province (grant no. J17KA141), the Medical and Health Technology Development Program in Shandong province (grant no. 2016WS0673), the Project of Traditional Chinese Medicine Technology Development Program in Shandong Province (2017-212), and the Science and Technology Development Program in Weifang (grant nos. 2017YX065 and 2016YX011).

Availability of data and materials

The datasets used during the present study are available from the corresponding author upon reasonable request.

Authors' contributions

JW and GT conceived and designed the study. GT, JB, JD and BZ performed the experiments. ZG and XS analyzed and interpreted the data. JW, ZG and BZ wrote the paper. XS, GT and BZ reviewed and edited the manuscript.

Ethics approval and consent to participate

All animal care and experimental protocols complied with the Animal Management Rules of the Ministry of Health of China and were approved by the Animal Research Ethics Committee (Weifang, China), approval no. 2017-025.

Patient consent for publication

Not applicable.

Competing interests

The authors declare that they have no competing interests.

References

1. Nakagawa H, Fujita M and Fujimoto A: Genome sequencing analysis of liver cancer for precision medicine. Semin Cancer Biol: Mar 29, 2018 (Epub ahead of print).
2. Sia D, Villanueva A, Friedman SL and Llovet JM: Liver cancer cell of origin, molecular class, and effects on patient prognosis. Gastroenterology 152: 745-761, 2017.
3. Karimi M, Ghasemi A, Sahandi Zangabad P, Rahighi R, Moosavi Basri SM, Mirshekari H, Amiri M, Shafaei Pishabad Z, Aslani A, Bozorgomid M, *et al*: Smart micro/nanoparticles in stimulus-responsive drug/gene delivery systems. Chem Soc Rev 45: 1457-1501, 2016.
4. Cervello M, Pitarresi G, Volpe AB, Porsio B, Balasus D, Emma MR, Azzolina A, Puleio R, Loria GR, Puleo S and Giammona G: Nanoparticles of a polyaspartamide-based brush copolymer for modified release of sorafenib: In vitro and in vivo evaluation. J Control Release 266: 47-56, 2017.
5. Lin Q, Bao C, Yang Y, Liang Q, Zhang D, Cheng S and Zhu L: Highly discriminating photorelease of anticancer drugs based on hypoxia activatable phototrigger conjugated chitosan nanoparticles. Adv Mater 25: 1981-1986, 2013.
6. Castro F, Pinto ML, Silva AM, Pereira CL, Teixeira GQ, Gomez-Lazaro M, Santos SG, Barbosa MA, Gonçalves RM and Oliveira MJ: Pro-inflammatory chitosan/poly(gamma-glutamic acid) nanoparticles modulate human antigen-presenting cells phenotype and revert their pro-invasive capacity. Acta Biomater 63: 96-109, 2017.
7. Liang X, Fang L, Li X, Zhang X and Wang F: Activatable near infrared dye conjugated hyaluronic acid based nanoparticles as a targeted theranostic agent for enhanced fluorescence/CT/photoacoustic imaging guided photothermal therapy. Biomaterials 132: 72-84, 2017.
8. Wu JL, Tian GX, Yu WJ, Jia GT, Sun TY and Gao ZQ: pH-Responsive Hyaluronic Acid-Based Mixed Micelles for the Hepatoma-Targeting Delivery of Doxorubicin. Int J Mol Sci 17: 364, 2016.
9. Sui J, Cui Y, Cai H, Bian S, Xu Z, Zhou L, Sun Y, Liang J, Fan Y and Zhang X: Synergistic chemotherapeutic effect of sorafenib-loaded pullulan-Dox conjugate nanoparticles against murine breast carcinoma. Nanoscale 9: 2755-2767, 2017.
10. Tamura R, Uemoto S and Tabata Y: Augmented liver targeting of exosomes by surface modification with cationized pullulan. Acta Biomater 57: 274-284, 2017.
11. Xiong H, Du S, Ni J, Zhou J and Yao J: Mitochondria and nuclei dual-targeted heterogeneous hydroxyapatite nanoparticles for enhancing therapeutic efficacy of doxorubicin. Biomaterials 94: 70-83, 2016.
12. Li K, Liu H, Gao W, Chen M, Zeng Y, Liu J, Xu L and Wu D: Mulberry-like dual-drug complicated nanocarriers assembled with apogossypolone amphiphilic starch micelles and doxorubicin hyaluronic acid nanoparticles for tumor combination and targeted therapy. Biomaterials 39: 131-144, 2015.
13. Han X, Dong X, Li J, Wang M, Luo L, Li Z, Lu X, He R, Xu R and Gong M: Free paclitaxel-loaded E-selectin binding peptide modified micelle self-assembled from hyaluronic acid-paclitaxel conjugate inhibit breast cancer metastasis in a murine model. Int J Pharm 528: 33-46, 2017.
14. Zhang H, Li W, Guo X, Kong F, Wang Z, Zhu C, Luo L, Li Q, Yang J, Du Y and You J: Specifically increased paclitaxel release in tumor and synergetic therapy by a hyaluronic acid-tocopherol nanomicelle. ACS Appl Mater Interfaces 9: 20385-20398, 2017.
15. Lin L, Cai M, Deng S, Huang W, Huang J, Huang X, Huang M, Wang Y, Shuai X and Zhu K: Amelioration of cirrhotic portal hypertension by targeted cyclooxygenase-1 siRNA delivery to liver sinusoidal endothelium with polyethylenimine grafted hyaluronic acid. Nanomedicine 13: 2329-2339, 2017.
16. Zhou Z, Li H, Wang K, Guo Q, Li C, Jiang H, Hu Y, Oupicky D and Sun M: Bioreducible cross-linked hyaluronic acid/calcium phosphate hybrid nanoparticles for specific delivery of siRNA in melanoma tumor therapy. ACS Appl Mater Interfaces 9: 14576-14589, 2017.
17. Fan J and Yang J: Preparation and characterization of a chitosan/galactosylated hyaluronic acid/heparin scaffold for hepatic tissue engineering. J Biomater Sci Polym Ed 28: 569-581, 2017.
18. Han X, Wang Z, Wang M, Li J, Xu Y, He R, Guan H, Yue Z and Gong M: Liver-targeting self-assembled hyaluronic acid-glycyrrhetinic acid micelles enhance hepato-protective effect of silybin after oral administration. Drug Deliv 23: 1818-1829, 2016.
19. Zhang L, Yao J, Zhou J, Wang T and Zhang Q: Glycyrrhetinic acid-graft-hyaluronic acid conjugate as a carrier for synergistic targeted delivery of antitumor drugs. Int J Pharm 441: 654-664, 2013.

20. Wang X, Gu X, Wang H, Sun Y, Wu H and Mao S: Synthesis, characterization and liver targeting evaluation of self-assembled hyaluronic acid nanoparticles functionalized with glycyrrhetinic acid. Eur J Pharm Sci 96: 255-262, 2017.
21. Dahlman JE, Kauffman KJ, Xing Y, Shaw TE, Mir FF, Dlott CC, Langer R, Anderson DG and Wang ET: Barcoded nanoparticles for high throughput in vivo discovery of targeted therapeutics. Proc Natl Acad Sci USA 114: 2060-2065, 2017.
22. Li J, Chen T, Deng F, Wan J, Tang Y, Yuan P and Zhang L: Synthesis, characterization, and in vitro evaluation of curcumin-loaded albumin nanoparticles surface-functionalized with glycyrrhetinic acid. Int J Nanomedicine 10: 5475-5487, 2015.
23. Lv Y, Li J, Chen H, Bai Y and Zhang L: Glycyrrhetinic acid-functionalized mesoporous silica nanoparticles as hepatocellular carcinoma-targeted drug carrier. Int J Nanomedicine 12: 4361-4370, 2017.
24. Qi WW, Yu HY, Guo H, Lou J, Wang ZM, Liu P, Sapin-Minet A, Maincent P, Hong XC, Hu XM and Xiao YL: Doxorubicin-loaded glycyrrhetinic acid modified recombinant human serum albumin nanoparticles for targeting liver tumor chemotherapy. Mol Pharm 12: 675-683, 2015.
25. Spaeth JR, Kevrekidis IG and Panagiotopoulos AZ: A comparison of implicit- and explicit-solvent simulations of self-assembly in block copolymer and solute systems. J Chem Phys 134: 164902, 2011.
26. Park K, Lee GY, Kim YS, Yu M, Park RW, Kim IS, Kim SY and Byun Y: Heparin-deoxycholic acid chemical conjugate as an anticancer drug carrier and its antitumor activity. J Control Release 114: 300-306, 2006.
27. Huang W, Wang W, Wang P, Tian Q, Zhang C, Wang C, Yuan Z, Liu M, Wan H and Tang H: Glycyrrhetinic acid-modified poly(ethylene glycol)-b-poly(gamma-benzyl l-glutamate) micelles for liver targeting therapy. Acta Biomater 6: 3927-3935, 2010.
28. Wu JL, Liu CG, Wang XL and Huang ZH: Preparation and characterization of nanoparticles based on histidine-hyaluronic acid conjugates as doxorubicin carriers. J Mater Sci Mater Med 23: 1921-1929, 2012.
29. Zhang C, Wang W, Liu T, Wu Y, Guo H, Wang P, Tian Q, Wang Y and Yuan Z: Doxorubicin-loaded glycyrrhetinic acid-modified alginate nanoparticles for liver tumor chemotherapy. Biomaterials 33: 2187-2196, 2012.
30. Chen H, Li M, Wan T, Zheng Q, Cheng M, Huang S and Wang Y: Design and synthesis of dual-ligand modified chitosan as a liver targeting vector. J Mater Sci Mater Med 23: 431-441, 2012.
31. Lee H, Mok H, Lee S, Oh YK and Park TG: Target-specific intracellular delivery of siRNA using degradable hyaluronic acid nanogels. J Control Release 119: 245-252, 2007.
32. Choi KY, Chung H, Min KH, Yoon HY, Kim K, Park JH, Kwon IC and Jeong SY: Self-assembled hyaluronic acid nanoparticles for active tumor targeting. Biomaterials 31: 106-114, 2010.
33. Qiu L, Li Z, Qiao M, Long M, Wang M, Zhang X, Tian C and Chen D: Self-assembled pH-responsive hyaluronic acid-g-poly((L)-histidine) copolymer micelles for targeted intracellular delivery of doxorubicin. Acta Biomater 10: 2024-2035, 2014.
34. Bastakoti BP, Liao SH, Inoue M, Yusa SI, Imura M, Nakashima K, Wu KC and Yamauchi Y: pH-responsive polymeric micelles with core-shell-corona architectures as intracellular anti-cancer drug carriers. Sci Technol Adv Mater 14: 044402, 2013.
35. Luo Z and Jiang J: pH-sensitive drug loading/releasing in amphiphilic copolymer PAE-PEG: Integrating molecular dynamics and dissipative particle dynamics simulations. J Control Release 162: 185-193, 2012.
36. Qiu L, Qiao M, Chen Q, Tian C, Long M, Wang M, Li Z, Hu W, Li G, Cheng L, *et al*: Enhanced effect of pH-sensitive mixed copolymer micelles for overcoming multidrug resistance of doxorubicin. Biomaterials 35: 9877-9887, 2014.
37. Du H, Liu M, Yu A, Ji J and Zhai G: Insight into the role of dual-ligand modification in low molecular weight heparin based nanocarrier for targeted delivery of doxorubicin. Int J Pharm 523: 427-438, 2017.
38. Di Y, Li T, Zhu Z, Chen F, Jia L, Liu W, Gai X, Wang Y, Pan W and Yang X: pH-sensitive and folic acid-targeted MPEG-PHIS/FA-PEG-VE mixed micelles for the delivery of PTX-VE and their antitumor activity. Int J Nanomedicine 12: 5863-5877, 2017.
39. Kobayashi T, Ishida T, Okada Y, Ise S, Harashima H and Kiwada H: Effect of transferrin receptor-targeted liposomal doxorubicin in P-glycoprotein-mediated drug resistant tumor cells. Int J Pharm 329: 94-102, 2007.
40. Iyer AK, Khaled G, Fang J and Maeda H: Exploiting the enhanced permeability and retention effect for tumor targeting. Drug Discov Today 11: 812-818, 2006.
41. Björnmalm M, Thurecht KJ, Michael M, Scott AM and Caruso F: Bridging Bio-Nano Science and Cancer Nanomedicine. ACS Nano 11: 9594-9613, 2017.
42. Wang J, Ma W, Guo Q, Li Y, Hu Z, Zhu Z, Wang X, Zhao Y, Chai X and Tu P: The effect of dual-functional hyaluronic acid-vitamin E succinate micelles on targeting delivery of doxorubicin. Int J Nanomedicine 11: 5851-5870, 2016.